

Lamellar crystal thickness transition of melt-crystallized isotactic polybutene-1 observed by small-angle X-ray scattering

Motoi Yamashita* and Minoru Kato

Department of Applied Chemistry, Ritsumeikan University, 1-1-1 Noji-higashi, Kusatsu, Shiga 525-8577, Japan.
Correspondence e-mail: motoi-y@is.ritsumei.ac.jpReceived 16 August 2006
Accepted 12 March 2007© 2007 International Union of Crystallography
Printed in Singapore – all rights reserved

The first-order long period L_1 , the second-order long period L_2 and lamellar crystal thickness l_c of isotactic polybutene-1 have been investigated for crystallization in the melt over a wide range (313.2 to 363.2 K) of crystallization temperatures by small-angle X-ray scattering experiments and density measurements. The long period L_1 shows a single linear dependence on inverse supercooling. The crystal thickness l_c , however, demonstrates two linear dependences on inverse supercooling and a transition from one dependence to the other has been observed around 338.2 K, where l_c becomes comparable with the radius of gyration R_g of the samples.

1. Introduction

In the crystallization of polymers, polymer chains in the form of random coils develop into double layer structures composed of folded chain crystals and amorphous layers. The nucleation theory by Hoffman *et al.* (Hoffman *et al.*, 1976; Hoffman & Miller, 1997) explains that the crystal thickness of polymers is determined kinetically, and gives the observed dependence of lamellar thickness l_c on supercooling $\Delta T = T_m^0 - T$ (T_m^0 is the equilibrium melting temperature, T is the crystallization temperature) by the following equation (l_c shows a single linear dependence on inverse supercooling, $1/\Delta T$):

$$l_c = \frac{A}{\Delta T} + \delta l \equiv l_c^* + \delta l, \quad (1)$$

where A and δl are constants. According to the theory, A is expressed as

$$A = \frac{2\sigma_e T_m^0}{\Delta h_f}, \quad (2)$$

Here, σ_e is the end-surface free energy per unit area of polymer crystals and Δh_f the heat of fusion per unit volume of the crystal phase. The first term $l_c^* = 2\sigma_e T_m^0 / \Delta h_f \Delta T$ in equation (1) represents the minimum lamellar thickness to keep the crystal thermodynamically stable and the second term corresponds to the driving force of crystallization. Hence, long period structures and crystal thicknesses of semicrystalline polymers reflect the processes of their structure formation.

Recently, Fu *et al.* (2001) observed a deviation from the nucleation theory in the temperature dependence of the crystal thickness of isotactic polybutene-1 (it-PB1) determined from electron density correlation analysis of small-angle X-ray scattering (SAXS) profiles. They observed that two different relationships exist between crystal thickness l_c and crystallization temperature T , and that a transition from one relationship to the other occurs, *i.e.*, l_c increases discontinuously accompanied by a morphological change of the crystals when l_c becomes comparable to the chain dimensions. They also showed that crystals with two different kinds of thicknesses co-exist around the transition temperatures.

To elucidate the influence of chain dimensions on the resultant lamellar long period structure, we have reinvestigated this transition in terms of more simple methods, using it-PB1 samples with a different molecular weight distribution from that used in the study by Fu *et al.* (2001). We have studied the temperature dependence of the first- and second-order long periods and lamellar crystal thicknesses of it-PB1 tetragonal crystals grown in the melt by SAXS experiments and crystallinity measurements. it-PB1 is a semicrystalline polyolefin with ethyl side groups. it-PB1 exhibits a stable trigonal form with 3/1 helical chains and a metastable tetragonal form with 11/3 helical chains as the most common structures, as shown in Table 1. Crystallization in the bulk melt under atmospheric pressure yields the tetragonal form (Turner-Jones, 1963). Due to the metastability of the tetragonal form, the solid–solid spontaneous transformation to the stable trigonal form then takes place over several days after cooling to room temperature (Natta *et al.*, 1960).

In this study, we again confirmed the two different temperature dependences of the crystal thickness l_c . We observed two linearities in the inverse supercooling dependence of l_c , which indicates that each of the two relationships still obeys the nucleation theory. We also observed an abnormality in the supercooling dependence of the second-order long period around 353.2 K. We are going to discuss possible mechanisms for the transition.

2. Experimental

2.1. Lamellar crystal thickness

The it-PB1 used in this study was purchased from Scientific Polymer Products. Weight- and number-averaged molecular weights determined with gel permeation chromatography (GPC) calibrated with polystyrene standard samples are $M_w = 277\,300$ and $M_n = 60\,340$, respectively.

We measured the density ρ of samples by a float and sink method using mixed solvents of water and ethanol at 298.2 K; the crystallinity φ was determined from the density using

$$\rho = \rho_c \varphi + \rho_a (1 - \varphi), \quad (3)$$

Table 1
Physical properties of it-PB1.

| | Unit-cell parameters | | | | Stem parameters | | Δh_i^\ddagger (J m ⁻³) | T_m^0 [‡] (K) | Space group | Chain conformation (monomers/turn) |
|-------------|----------------------|--------------|--------------|---|-----------------|------------|---|-----------------------------|--------------|---------------------------------------|
| | a_0 (Å) | b_0 (Å) | c_0 (Å) | ρ^\dagger (g cm ⁻³) | a (Å) | b (Å) | | | | |
| Trigonal§ | 17.7 | 17.7 | 6.5 | 0.96 | 5.1 | 8.85 | 1.35×10^8 | 397.2 | $\bar{R}3c$ | 3/1 |
| Tetragonal¶ | 14.6 | 14.6 | 21.2 | 0.888 | 7.3 | 7.3 | 1.09×10^8 | 409.2 | $\bar{P}4b2$ | 11/3 |
| Amorphous | | | | 0.87 | | | | | | |

† Miller (1999). ‡ Leute & Dollhopf (1983). § Natta *et al.* (1960). ¶ Tashiro *et al.* (1998).

where ρ_c and ρ_a are the densities of the crystalline and amorphous phases, respectively, listed in Table 1.

SAXS photographs were taken with a SAXS camera (camera length 414 mm) in vacuum to obtain lamellar long periods, using an imaging plate system (Rigaku R-AXIS DSII). Nickel-filtered Cu $K\alpha$ radiation was used, generated at 50 kV and 140 mA. After the subtraction of the background intensity, isotropic two-dimensional data were circularly averaged to obtain one-dimensional data and corrected for the Lorentz factor. The first- and second-order reflections were separated by fitting SAXS profiles with Gaussian–Lorentzian product functions. Application of Bragg’s law to the scattering peak centers was used to calculate the first- and second-order long periods, L_1 and L_2 . The lamellar crystal thickness l_c was estimated using the equation $l_c = \phi L_1$.

Films of it-PB1 of about 500 μm thickness were sandwiched between aluminium foil and melted at 423.2 K for 3 min in an oven, transferred quickly to a hot stage (Mettler FP82) and kept at a crystallization temperature between 313.2 and 363.2 K. The films crystallized were aged at room temperature for 10 d and used for SAXS and density measurements. After 10 d of aging at room temperature, the tetragonal crystals transform into the trigonal form without changing their stacked lamellae structure and overall mass degree of crystallinity. Since the crystal density of the trigonal form is larger than that of the tetragonal form, the SAXS intensity is much enhanced after 10 d. We determined l_c of the aged samples, then calculated l_c of the as-crystallized tetragonal samples from the observed values of l_c of the aged samples assuming that $l_c(\text{as-crystallized}) = l_c(\text{aged})/1.12$. This assumption is based on the fact that the

tetragonal–trigonal transformation involves an extension of the 11/3 helical conformation (tetragonal form) into the 3/1 helix (trigonal form). The ratio between the axial repeating units of this conformation is 1.12.

2.2. Identification of crystal structures

Wide-angle X-ray scattering (WAXS) was performed to identify crystal structures. Nickel-filtered Cu $K\alpha$ radiation was used, generated at 35 kV and 40 mA. The system and procedure used for data acquisition and analysis were the same as those used for SAXS experiments.

3. Results

3.1. Crystal structures from WAXS and TEM

We confirmed by WAXS measurements that samples immediately after the crystallization are in the tetragonal form (Fig. 1). Hence the observed crystallinity and lamellar crystal thickness reflect those of tetragonal crystals. Samples stored at room temperature for 10 d exhibited peaks characteristic of the trigonal form.

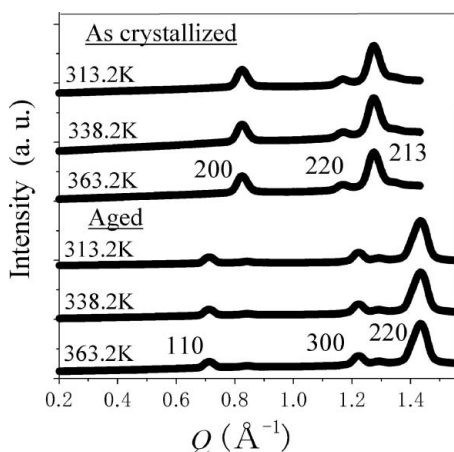


Figure 1
WAXS profiles of it-PB1 crystallized at 313.2, 338.2 and 363.2 K plotted against the modulus of the scattering vector Q . ($Q = 4\pi\lambda^{-1}\sin\theta$, θ is half the scattering angle, λ is the wavelength used.) The profiles for samples as crystallized and aged are plotted. Peaks shown in the plots of as crystallized samples are indexed with the 200, 220, 213 reflections of the tetragonal form; peaks exhibited in the plots of the aged samples are indexed with the 110, 300, 220 reflections of the trigonal form.

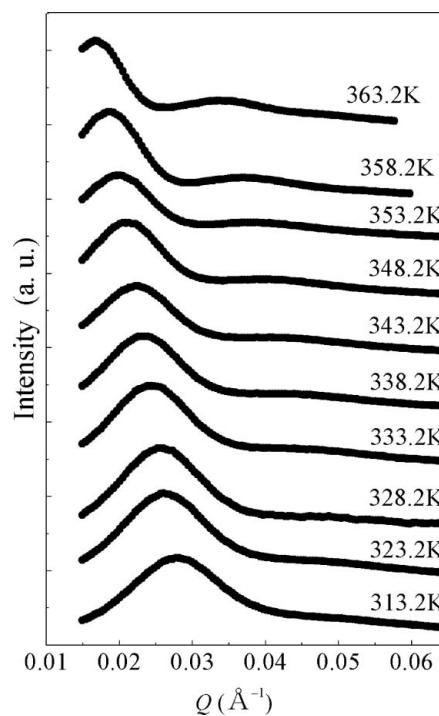


Figure 2
SAXS profiles for it-PB1 samples crystallized at temperatures from 313.2 to 363.2 K. The profiles have been shifted vertically for clarity.

Table 2

Results of SAXS and crystallinity measurements.

T_c = crystallization temperature, L_1 = the first-order long period, L_2 = the second-order long period, φ = crystallinity, l_c = lamellar crystal thickness. The l_c data are estimated values of as-crystallized samples before aging; they were derived assuming $l_c(\text{as-crystallized}) = l_c(\text{aged})/1.12$. (See the text.)

| T_c (K) | L_1 (Å) | L_2 (Å) | L_2/L_1 | φ (%) | l_c (Å) |
|-----------|-----------|-----------|-----------|---------------|-----------|
| 313.2 | 222 | 125 | 0.563 | 46.7 | 92.7 |
| 323.2 | 237 | 130 | 0.547 | 46.1 | 97.6 |
| 328.2 | 247 | 133 | 0.538 | 46.6 | 102 |
| 333.2 | 258 | 136 | 0.526 | 46.7 | 106 |
| 338.2 | 267 | 141 | 0.530 | 49.2 | 117 |
| 343.2 | 281 | 146 | 0.521 | 51.7 | 130 |
| 348.2 | 297 | 158 | 0.530 | 51.7 | 137 |
| 353.2 | 319 | 170 | 0.534 | 54.2 | 154 |
| 358.2 | 334 | 171 | 0.511 | 54.2 | 162 |
| 363.2 | 368 | 182 | 0.495 | 55.9 | 184 |

3.2. Lamellar crystal thickness

Fig. 2 shows the Lorentz-corrected SAXS profiles of the samples. First- and second-order reflections were observed in the wide range of crystallization temperatures from 313.2 to 363.2 K. Table 2 lists the results of SAXS and density measurements: crystallization temperatures, the values of the first- and second-order long periods, the ratios of the second-order long period to the first-order long period, the degrees of crystallinity and the lamellar crystal thicknesses.

Fig. 3 shows the first-order long period L_1 and second-order long period L_2 as a function of the inverse supercooling, $1/\Delta T$. ($\Delta T = T_m^0 - T$; the equilibrium melting temperature T_m^0 is 397.2 K for the iPPB1 tetragonal phase, as given in Table 1.) The $1/\Delta T$ dependence of L_1 demonstrates a single linearity over the whole temperature range investigated. For the $1/\Delta T$ dependence of L_2 , on the contrary, a shoulder is observed around $1/\Delta T = 0.0227$, which corresponds to a crystallization temperature $T = 353.2$ K.

Fig. 4 shows the lamellar crystal thickness l_c plotted against $1/\Delta T$. The dependence deviates from a single linearity. Two linear relationships between l_c and $1/\Delta T$ can be observed, one in the low ΔT range ($1/\Delta T = 0.018-0.030 \text{ K}^{-1}$; this corresponds to $T = 363-343$ K) and the other in the high ΔT range ($1/\Delta T = 0.012-0.016 \text{ K}^{-1}$; this corresponds to $T = 333-313$ K). When $1/\Delta T$ increases from the high

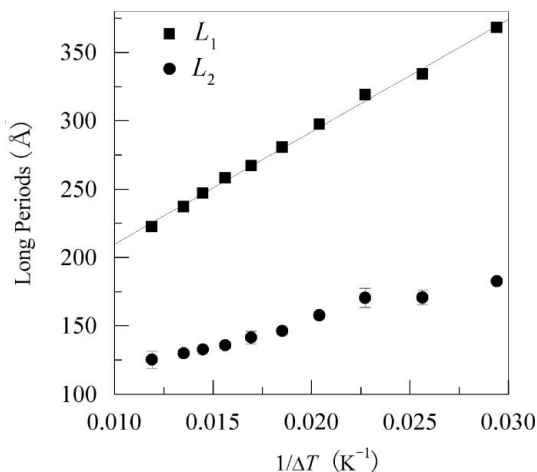


Figure 3
The first-order long period L_1 and the second-order long period L_2 as a function of the inverse supercooling, $1/\Delta T$.

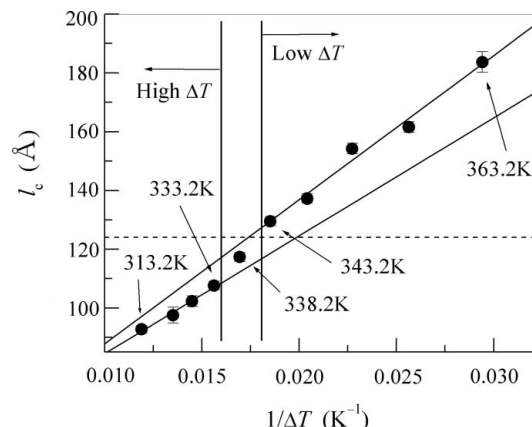


Figure 4
Lamellar crystal thickness l_c as a function of the inverse supercooling, $1/\Delta T$. The broken line represents the radius of gyration R_g .

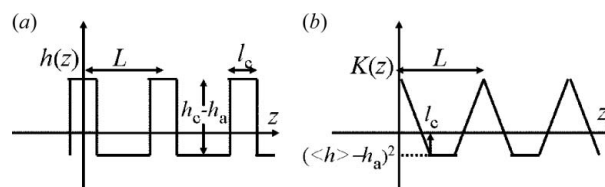


Figure 5
(a) Electron density distribution function $h(z)$ and (b) the related correlation function $K(z)$ for a strictly periodic two phase system.

ΔT range to the low ΔT range, l_c moves up from the lower line to the upper line in Fig. 4. This is in agreement with the observation reported by Fu *et al.* (2001). At $1/\Delta T = 0.017$, l_c lies in the middle of the two linearities, which suggests a transition state between the two linear relationships. According to equations (1) and (2), the extrapolation to $1/\Delta T = 0 \text{ K}^{-1}$ of the straight lines in Fig. 4 gives the values of δl_c to be $38.8 \pm 8.4 \text{ Å}$ for the low ΔT range and $44.3 \pm 4.8 \text{ Å}$ for the high ΔT range. The slopes give the values of $2\sigma_c T_m^0 / \Delta h_f$ to be $(4.90 \pm 0.39) \times 10^3 \text{ Å K}$ for the low ΔT range and $(4.01 \pm 0.35) \times 10^3 \text{ Å K}$ for the high ΔT range; σ_c is estimated as $(6.73 \pm 0.49) \times 10^{-2} \text{ J m}^{-2}$ for the low ΔT range and $(5.51 \pm 0.48) \times 10^{-2} \text{ J m}^{-2}$ for the high ΔT range, using the values of Δh_f and T_m^0 given in Table 1. Chain folding free energies $q = 2ab\sigma_c$ (a and b represent the height and width of a stem, respectively; the values are shown in Table 1) are calculated as $(7.17 \pm 0.52) \times 10^{-20} \text{ J stem}^{-1}$ for the low ΔT range and $(5.87 \pm 0.51) \times 10^{-20} \text{ J stem}^{-1}$ for the high ΔT range.

4. Discussion

First, we will discuss the temperature and crystallinity dependence of L_1 and L_2 . For simplicity, we consider strictly periodic two-phase systems as reviewed by Strobl & Schneider (1980) and assume our crystallized samples to be composed of ensembles of many different strictly periodic structures with different long periods. A periodic structure shows an electron density distribution $h(z)$ as indicated in Fig. 5(a). It can be described by specifying the long period L , the crystal thickness l_c and the electron density of the crystal and amorphous phases, h_c and h_a . Here, and in the following, we choose a crystallinity $\varphi = l_c/L < 0.5$.

The correlation function $K(z)$ is given by the following expressions:

$$K(z) = K_a(z) - (\langle h \rangle - h_a)^2$$

$$K_a(z) = \int_{-\Delta/2}^{\Delta/2} [h(z') - h_a][h(z' + z) - h_a] dz' \quad (4)$$

Here Δ denotes the average range for z' . $K_a(z)$ is calculated as follows:

$$K_a(z) = (h_c - h_a)^2(d - z)/L \quad \text{if } |z| < d$$

$$= 0 \quad \text{if } d < |z| < |L - d| \quad (5)$$

$$K_a(z + L) = K_a(z).$$

Equations (4) and (5) give the profile of $K(z)$ as shown in Fig. 5(b). The scattering intensity distribution function $S(Q)$ is given as follows:

$$S(Q) = \frac{2}{4\pi Q^2} (2\pi)^2 \int_{-\infty}^{\infty} \exp(iQz) K(z) dz. \quad (6)$$

In periodic systems with long period L , the first- and second-order scattering is observed where the modulus of the scattering vector Q takes values of $2\pi/L$ and $4\pi/L$, respectively, referring to Bragg's equation $\lambda = 2d \sin \theta$ (θ is half the scattering angle). The Lorentz-corrected first- and second-order scattering intensity is given as $4\pi Q^2 S(2\pi/L)$ and $4\pi Q^2 S(4\pi/L)$, respectively, and is readily calculated as follows:

$$S\left(\frac{2\pi}{L}\right) \propto 1 - \cos\left(2\pi \frac{l_c}{L}\right) = 1 - \cos 2\pi\phi \equiv S_1(\phi) \quad (7)$$

$$S\left(\frac{4\pi}{L}\right) \propto 1 - \cos\left(4\pi \frac{l_c}{L}\right) = 1 - \cos 4\pi\phi \equiv S_2(\phi).$$

For samples with $\phi > 0.5$, we can apply all the equations after making the replacements of $\phi \rightarrow 1 - \phi$ and $h_c \leftrightarrow h_a$, and we obtain

$$S\left(\frac{2\pi}{L}\right) \propto 1 - \cos\left(2\pi \frac{L - l_c}{L}\right) = 1 - \cos[2\pi(1 - \phi)] \equiv S_1(\phi) \quad (8)$$

$$S\left(\frac{4\pi}{L}\right) \propto 1 - \cos\left(4\pi \frac{L - l_c}{L}\right) = 1 - \cos[4\pi(1 - \phi)] \equiv S_2(\phi).$$

This follows from Babinet's reciprocity theorem. Fig. 6 shows the ϕ dependences of $S(2\pi/L) \equiv S_1$ and $S(4\pi/L) \equiv S_2$. The S_1 value becomes a maximum at $\phi = 0.5$ while S_2 takes a minimal value 0 at $\phi = 0.5$.

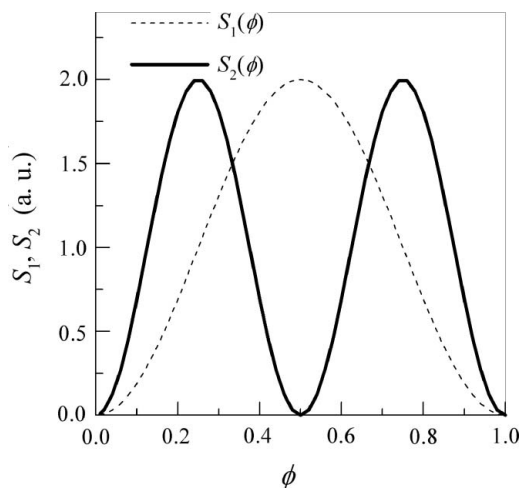


Figure 6 Crystallinity ϕ dependences of the first- and second-order scattering intensity S_1 and S_2 .

We then introduce a crystal thickness distribution function $F_c(l_c)$, assuming l_a to be a fixed value at a given temperature. The distribution function of the long period is given as $F_L(L) = F_c(L - l_a)$. $F_c(l_c)$ is considered to possess an asymmetric profile as given in Fig. 7(a), since l_c has a lower bound $l_c^* = 2\sigma_c T_m^0 / \Delta h_f \Delta T$ for lamellar crystals to keep themselves thermodynamically stable. We discuss here the scattering intensity distribution in real space L instead of Q space. The first- and second-order scattering intensity distribution from ensembles of periodic structures with many different long periods is given by $S_1(\phi)F_L(L)$ and $S_2(\phi)F_L(L)$, respectively. The peak position L'_1 of $S_1(\phi)F_L(L)$ corresponds to the first-order scattering peak position in Q space. Hence, L'_1 is equal to L_1 . On the other hand, if we put L'_2 to be the peak position of $S_2(\phi)F_L(L)$, $L'_2/2$ corresponds to the second-order peak position in Q space. Hence, L_2 is equal to $L'_2/2$. Around the range of observed ϕ , $S_1(\phi)$ can roughly be taken to be constant and L_1 is roughly equal to the peak position of $F_L(L)$. On the contrary, $S_2(\phi)$ becomes close to 0 around $\phi = 0.5$, i.e. $L = 2l_a$. Distribution of L far from $L = 2l_a$ largely contributes to the second-order scattering and contribution from the range around $2l_a$ is negligible.

At ϕ slightly smaller than 0.5, the main part of the distribution which lies around the $F_L(L)$ peak does not contribute to the second-order scattering (Fig. 7b). Only the long distribution 'tail' which locates in the range of L sufficiently larger than $2l_a > L_1$ contributes to L_2 . Hence, the second-order scattering is weak and $S_2(\phi)F_L(L)$ has a peak around $L'_2 > L'_1 = L_1$; L_2/L_1 becomes larger than 1/2. With increasing crystallization temperature the crystallinity ϕ increases, and the distribution of L shifts to a larger value of L . The distribution,

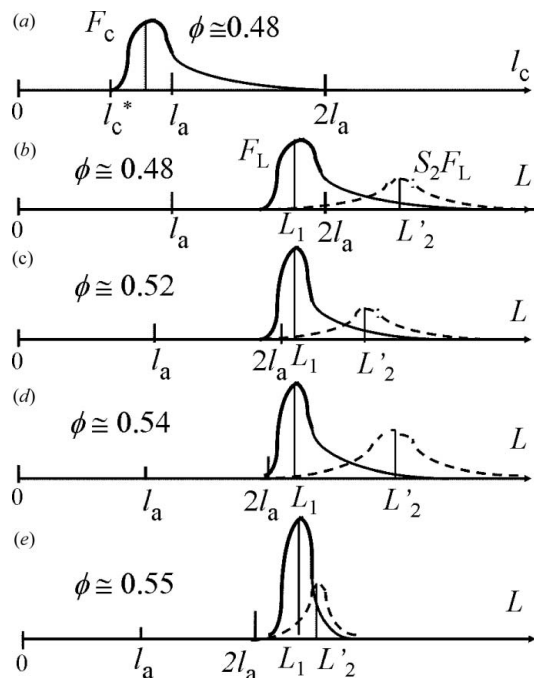


Figure 7 (a) Speculated profiles of the crystal thickness distribution function $F_c(l_c)$ at $\phi \approx 0.48$, (b)–(e) long period distribution functions $F_L(L)$ (solid lines) and second-order scattering intensity distribution functions $S_2(\phi)F_L(L)$ (broken lines) at several different crystallinity ϕ values. The shapes of these asymmetric functions were estimated from the function $(l_c - l_c^*) \exp[-B(l_c^* + \delta l)/kT]$ defined in the range $l_c > l_c^*$. (B is a constant.) The first factor represents the driving force of crystallization and the second factor represents the barrier for chain folding. The convergence of distribution with increasing temperature can be accounted for by the second factor.

however, also converges to around L_1 (Fig. 7c). The distribution tail becomes shorter, which makes L_2/L_1 decrease almost monotonically toward 0.5. Around $\varphi \approx 0.55$ (Fig. 7d), the main part of the distribution of L is considered to shift to the region $L > 2l_a$. A considerable part of the distribution of L larger than L_1 contributes to the second-order scattering, which makes L_2/L_1 larger again. This can account for the shoulder around $1/\Delta T = 0.0227$, which corresponds to $T = 353$ K. At higher crystallization temperatures, the distribution is considered to become much more converged around L_1 (Fig. 7e). The distribution tail located at $L > L_1$ becomes much smaller and L_2/L_1 approaches 1/2 again. To summarize, we can speculate that the shoulder observed in the L_2 vs $1/\Delta T$ plot is caused by the asymmetric distribution of L when it passes through $2l_a$, converging on itself.

We next consider the transition observed in the l_c vs $1/\Delta T$ plot. We observed two different dependences of l_c on $1/\Delta T$ and the transition between them. This is consistent with the observation by Fu *et al.* (2001). On the other hand, l_c depends linearly on $1/\Delta T$ in each of the low and high supercooling ranges, which is in accordance with the nucleation theory. The growth mechanisms described by the nucleation theory still seem to be working in each of the low and high supercooling ranges. Below we are going to analyze the transition according to the hypothesis proposed by Fu *et al.* and show that one of the results obtained in this work can not be explained by their model. Then we will present a simple model that can account for the transition.

Polymer chains are elongated along the crystal-melt interface before they become incorporated into the crystal phase. If the crystal thickness is smaller than the chain dimensions in the melt, Fu *et al.* (2001) assumed that crystallization does not necessary need a chain disentangling; the entanglements can be shifted into the amorphous regions, where they can be accumulated together with the other noncrystallizable chain parts such as end groups and stereodeflects. An estimation of the chain dimensions in the melt is the radius of gyration R_g . Then, the condition for crystallization without disentangling can be obtained as follows:

$$l_c \leq R_g. \quad (9)$$

If this condition is not satisfied, *i.e.* if the crystal thickness is larger than R_g , they proposed that the chain needs to be disentangled to crystallize.

For Gaussian chains, R_g and the mean-squared end-to-end distance R_0 are related by the following equation:

$$R_g^2 = \frac{R_0^2}{6}. \quad (10)$$

R_0 can be calculated using the characteristic ratio C_∞ as

$$R_0^2 = C_\infty a_b^2 N. \quad (11)$$

Here, a_b^2 represents the sum of squares of the lengths of the backbone bonds in one monomer unit and N is the degree of polymerization.

For it-PB1, C_∞ is given as 18.0 in the literature (Kurata & Tsunashima, 1999); a_b^2 is 4.74 \AA^2 . The value N is calculated to be 1078 from the number-averaged molecular weight and R_g is determined to be 124 \AA . This value is roughly in agreement with the crystal thickness 117 \AA at $T = 338.2 \text{ K}$ ($1/\Delta T = 0.017$), which is the temperature of the crystal thickness transition observed in Fig. 4. The agreement supports the observations by Fu *et al.* (2001). The hypothesis that chain dimensions could influence the process of crystal growth seems to be right.

However, the model by Fu *et al.* (2001) can not explain the change in the slope of the l_c vs $1/\Delta T$ plot. The two linearities we observed in

the $1/\Delta T$ dependence of l_c also indicate that the dependences obey the nucleation theory in each of the high and low ΔT ranges. The slope of the l_c vs $1/\Delta T$ plot is proportional to the end surface free energy σ_e of crystals, *i.e.* it reflects the free energy $q = 2ab\sigma_e$ of a chain folding. The q value determined from the low ΔT range is larger than that determined from the high ΔT range by $1.30 \times 10^{-20} \text{ J stem}^{-1}$, which amounts to 22% of the q value in the high ΔT range. The difference can not be explained only by whether disentanglement of chain molecules works or not, because disentanglement itself changes neither the energy of chain folding nor the conformational entropy of polymer chain. When chains are elongated beyond R_g the envelope of the volume occupied by the chains can be elongated and deformed, causing the loss of conformational entropy of the chains. The reduced entropy, however, will be observed as the lateral surface free energy, not the end surface free energy. This can be reasonably treated within the nucleation theory (Hoffman & Miller, 1997).

Another candidate for the mechanisms causing the change of the slope in the l_c vs $1/\Delta T$ plot is the change of chain folding manner caused by kinetic roughening. it-PB1 tetragonal crystals have a faceted morphology indicative of flat growth fronts on the molecular scale at lower ΔT , while they present a rounded morphology with a kinetically roughened growth front on the molecular scale (Yamashita *et al.*, 2004, 2007). In faceted crystals of the tetragonal phase, the chain folding direction is restricted to that parallel to the (100) growth front within each (100) sector since step propagation occurs along the (100) growth front during the crystallization process. A chain can fold from one site in the lattice to its two adjacent sites along the (100) plane. On the contrary, in kinetically roughened crystals, the chain folding direction is no longer restricted to (100) directions; a chain can fold into at least eight neighboring sites. With increasing temperature, the growth front changes from rounded to faceted morphology, which reduces the number of re-entrant sites from eight to two. Reduced re-entrant sites cause the reduction of the configurational entropy of the re-entrant sites and the conformational entropy of a folded chain, and these factors could account for the difference between the chain folding free energy values. The entropy of chain re-entrant sites for faceted and kinetically roughened growth fronts are estimated to be $k \ln 2 \text{ stem}^{-1}$ and $k \ln 8 \text{ stem}^{-1}$, respectively; the reduction of chain re-entrant sites is calculated to be $2k \ln 2$. This corresponds to the free energy difference of $6.47 \times 10^{-21} \text{ J stem}^{-1}$ at 338.2 K . This value is half the difference between the q values, $13.0 \times 10^{-21} \text{ J stem}^{-1}$; if we assume the reduction of the conformational entropy to have the same order of magnitude as that of the configurational entropy of re-entrant sites, we can explain the difference between the q values.

In our previous work, we determined the kinetic roughening temperature to be around 358.2 K (Yamashita *et al.*, 2004). This is not in agreement with the observed temperature of the thickness transition, 338.2 K . However, we also observed (100) sector boundaries in kinetically roughened crystals at 358.2 K . The existence of sector boundaries indicates that the crystals have a considerable fraction of (100) folding even in the kinetically roughened state. This is considered to be due to the fact that the surface nucleation process is still alive and step propagation along the (100) direction is working on a kinetically roughened growth front, since the growth front is not thermally roughened. If we assume that the fraction of (100) folding undergoes a large decrease in the temperature range of 333.2 – 343.2 K , we can account for the transition temperature in the $1/\Delta T$ dependence of l_c . To confirm our hypothesis, we need to observe the (100) sector boundaries disappearing in this temperature range.

Although the second model described above is rather trivial, it seems more probable because it can explain the change in q without

any large changes in the crystallization mechanisms. Experiments on the crystallization behaviour are still insufficient to determine the mechanisms of transition. In particular, a more precise investigation of the crystallization kinetics and the morphology of growth shape in the high ΔT range is deemed necessary.

5. Conclusion

We observed the two temperature dependences of lamellar crystal thickness l_c and the transition from one dependence to the other reported by Fu *et al.* (2001) in the crystallization of the it-PB1 tetragonal phase with a different molecular weight by means of more simple methods. We determined the first-order long period L_1 and the second-order long period L_2 along with the lamellar crystal thickness l_c of tetragonal crystals of it-PB1 grown in the melt from SAXS experiments and density measurements over a wide range of crystallization temperatures T from 313.2 to 363.2 K. The $1/\Delta T$ dependence of L_1 demonstrated a single linearity over the whole temperature range investigated while that of L_2 showed a shoulder around $1/\Delta T = 0.0227$, which corresponds to $T = 353.2$ K. The shoulder could be attributed to the asymmetric distribution of l_c converging with increasing temperature and the increase of crystallinity accompanied by increasing crystallization temperature. The dependence of l_c on $1/\Delta T$ presented two linearities and the transition from one dependence to the other was observed around $T = 338.2$ K, where l_c becomes roughly in agreement with the radius of gyration R_g of the samples we used. Each of the two dependences obeys the nucleation theory in the high and low ΔT ranges. The chain folding free energy q determined from the low ΔT range is larger than that determined from the high ΔT range by 1.30×10^{-20} J stem $^{-1}$. The model proposed by Fu *et al.* (2001) can not account for the change in the difference between the q values, while it can roughly explain the transition temperature. The difference can be roughly explained by considering the change in chain folding directions caused by kinetic

roughening without any large change of crystallization mechanisms as assumed by Fu *et al.* (2001).

The authors express their sincere thanks to Mr Masada (Tokuyama Corporation) for GPC measurements, Professor Sawamura (Ritsumeikan University) and Dr Matsuo (Ritsumeikan University) for their kind instruction in the density measurement technique, Professor Nakamura (Ritsumeikan University) for help with the instrumentation used for sample preparation, and Mr Mori (Ritsumeikan University) and Mr Kudo (Ritsumeikan University) for their kind instruction in software used for SAXS profile analysis. This work was partially supported by 'Academic Frontier' Project from MEXT, 2004–2008.

References

- Fu, Q., Heck, B., Strobl, G. & Thoman, Y. (2001). *Macromolecules*, **34**, 2502–2511.
- Hoffman, J. D., Davis, G. T. & Lauritzen, J. I. Jr (1976). *Treatise on Solid State Chemistry*, edited by N. B. Hannay, pp. 497–614. New York: Plenum.
- Hoffman, J. D. & Miller, R. L. (1997). *Polymer*, **38**, 3151–3212.
- Kurata, M. & Tsunashima, Y. (1999). *Polymer Handbook*, edited by J. Brandrup & E. H. Immergut, Vol. VI, pp. 48–49. New York: Wiley Interscience.
- Leute, U. & Dollhopf, W. (1983). *Colloid Polym. Sci.* **261**, 299–305.
- Miller, R. L. (1999). *Polymer Handbook*, edited by J. Brandrup & E. H. Immergut, Vol. VI, pp. 7–8. New York: Wiley Interscience.
- Natta, G., Corradini, P. & Bassi, I. W. (1960). *Nuovo Cimento Suppl.* **15**, 52–67.
- Starkweather, H. W. Jr & Jones, G. A. (1986). *J. Polym. Sci. Part B Polym. Phys.* **24**, 1509–1514.
- Strobl, G. & Schneider, M. (1980). *J. Polym. Sci. Polym. Phys. Ed.* **18**, 1343–1359.
- Tashiro, K., Saiani, A., Miyashita, S., Chatani, Y. & Tadokoro, H. (1998). *Polym. Prepr. Jpn.* **47**, 3869–3870.
- Turner-Jones, A. (1963). *J. Polym. Sci. Part B Polym. Lett.* **1**, 455.
- Yamashita, M., Hoshino, A. & Kato, M. (2007). *J. Polym. Sci. Part B Polym. Phys.* **45**, 684–697.
- Yamashita, M., Miyaji, H., Izumi, K. & Hoshino, A. (2004) *Polym. J.* **36**, 226–237.